Tunable magnetic ordering through cation selection in entropic spinel oxides

Brianna Musicó,[1] Quinton Wright,[1] T. Zac Ward,[2] Alexander Grutter,[3] Elke Arenholz,[4] Dustin Gilbert,[1] David Mandrus,[1] and Veerle Keppens[1,*]

[1]*Joint Institute for Advanced Materials, Department of Materials Science and Engineering, University of Tennessee-Knoxville, Tennessee 37996-4545, USA*

[2]*Materials Science and Technology Division, Oak Ridge National Laboratory, Oak Ridge, Tennessee 37831, USA*

[3]*NIST Center for Neutron Research, National Institute of Standards and Technology, Gaithersburg, Maryland 20899-6102, USA*

[4]*Advanced Light Source, Lawrence Berkeley National Laboratory, Berkeley, California 94720, USA*

(Received 18 June 2019; published 21 October 2019)

Twelve multicomponent spinels, comprised of (Mg, Cr, Mn, Co, Fe, Ni, Cu, and/or Zn)(Cr, Fe, or Al)$_2$O$_4$, were prepared using solid state synthesis methods, resulting in nine homogenous, single phase samples with a Fm-3m structure, and three samples with multiple phases. Using dc magnetometry in conjunction with x-ray diffraction, scanning electron microscopy with energy dispersive x-ray spectroscopy, and x-ray absorption spectroscopy, the effects of multicomponent material design on the structural, magnetic, and chemical properties are explored. The ferritic spinel high-entropy oxide (HEO) samples show high-temperature ferrimagnetic transitions and both ferritic and chromium-based HEO spinel samples show evidence of low-temperature antiferromagnetic ordering. Blocking temperatures are evident in some samples and magnetic transition temperatures are reported. Constituent valence states and temperature dependent valence is described for the example case of $(Mg_{0.2}Fe_{0.2}Co_{0.2}Ni_{0.2}Cu_{0.2})Cr_2O_4$, including the unexpected presence of Cr^{4+}, indicating a 2–4 type spinel configuration. Valence trends for two ferritic HEO spinels are also discussed. Some of these compositions are synthesized for the first time and this work provides an investigation into the magnetic properties of the novel class of cubic spinel multicomponent oxides showing interesting behavior that warrants further investigation.

DOI: 10.1103/PhysRevMaterials.3.104416

I. INTRODUCTION

High-entropy alloys (HEAs) have been widely studied since their inception into materials research in 2004 making multicomponent systems an avenue for achieving and tuning a variety of physical properties [1]. In 2015 the field of multicomponent materials expanded into ceramic systems by introducing entropy stabilized oxides (ESOs), expanding the opportunities for functional materials, predicated on the basis of exaggerated substitution by populating a single site or sublattice with multiple cations [2]. Also termed high-entropy oxides (HEOs), these materials offer significant opportunities for functional material applications, but are exceedingly challenging to design as a result of their intrinsic disorder and highly localized chemical environments. While first realized with a rocksalt structure, HEO material synthesis has expanded to include perovskite and fluorite structures [3–7]. Due to the presence of multiple metallic elements in many HEO materials, they hold promise for a range of applications including rare-earth free permanent magnets and magnetic functional devices, however, magnetic properties have only recently started to be considered within these systems. The investigation into the exchange bias phenomena, reported in a rock salt HEO with varying concentration of Co, showed that the unique properties of HEO materials can be utilized to tailor the engineering of magnetic functional phenomena in oxide thin films [8]. Recently the dc and ac magnetometry and Mössbauer spectra of a few rare-earth and transition metal HEO perovskites (Gd, La, Nd, Sm, and/or Y)(Co, Cr, Fe, Mn, and/or Ni)O$_3$ type, which showed a relationship between the magnetic exchange and the disorder within the chemically complex compositions of this novel material class with a predominant antiferromagnetic behavior with small ferromagnetic contribution [9].

The spinel structure offers unique opportunities as a multicomponent system due to its large and complex unit cell, which consists of 32-anion sites, surrounded by 24-cations organized in both octahedral and tetrahedral cages. Furthermore, spinels offer significant opportunities for magnetic applications in, for example, biomedical [10] and data storage [11] technologies, motivating a multitude of works exploring the synthesis and functional properties of binary and ternary spinels [12]. The energetic preference of these tetrahedral or octahedral occupancies for many metal species in binary and ternary spinels is known and reported, but entropic contributions in multicomponent systems could overcome these to create a more random mixed occupancy distribution of multivalent cation species and subsequently interesting properties. Dabrowa *et al.* have reported the successful synthesis of a $(Cr_{0.2}Mn_{0.2}Fe_{0.2}Co_{0.2}Ni_{0.2})_3O_4$ high-entropy spinel, demonstrating the practicality of this approach [13]. Only recently has the magnetic behavior of $(Cr_{0.2}Mn_{0.2}Fe_{0.2}Co_{0.2}Ni_{0.2})_3O_4$ been investigated showing ferrimagnetic behavior at room temperature with magnetization dependent on crystallite size and subsequent exchange interaction [14]. Our work presents

*Corresponding author: vkeppens@utk.edu

TABLE I. Summary of the compositions synthesized and investigated in this study along with their processing temperatures.

Name	Composition	Heat Treatment		Single Phase
		Calcine	Sinter	
F1	$(Mg_{0.2}Fe_{0.2}Co_{0.2}Ni_{0.2}Cu_{0.2})Fe_2O_4$	-	1250 °C	Yes
F3	$(Mg_{0.2}Co_{0.2}Ni_{0.2}Cu_{0.2}Zn_{0.2})Fe_2O_4$	-	1250 °C	Yes
F4	$(Mg_{0.2}Mn_{0.2}Co_{0.2}Ni_{0.2}Cu_{0.2})Fe_2O_4$	950 °C	1250 °C	Yes
F5	$(Mn_{0.2}Fe_{0.2}Co_{0.2}Ni_{0.2}Cu_{0.2})Fe_2O_4$	950 °C	1250 °C	Yes
F6	$(Cr_{0.2}Mn_{0.2}Fe_{0.2}Co_{0.2}Ni_{0.2})_3O_4$[a]	-	1250 °C	Yes
F7	$(Mn_{0.2}Fe_{0.2}Co_{0.2}Ni_{0.2}Cu_{0.2})_3O_4$	950 °C	1250 °C	No
F8	$(Mg_{0.2}Fe_{0.2}Co_{0.2}Ni_{0.2}Cu_{0.2})_3O_4$	-	1250 °C	No
S1	$(Mg_{0.2}Co_{0.2}Ni_{0.2}Cu_{0.2}Zn_{0.2})Al_2O_4$	-	1600 °C	Yes
C1	$(Mg_{0.2}Co_{0.2}Ni_{0.2}Cu_{0.2}Zn_{0.2})Cr_2O_4$	-	1250 °C	Yes
C2	$(Mg_{0.2}Fe_{0.2}Co_{0.2}Ni_{0.2}Cu_{0.2})Cr_2O_4$	-	1250 °C	Yes
C3	$(Mg_{0.2}Mn_{0.2}Co_{0.2}Ni_{0.2}Cu_{0.2})Cr_2O_4$	950 °C	1250 °C	Yes
C4	$(Mn_{0.2}Fe_{0.2}Co_{0.2}Ni_{0.2}Cu_{0.2})Cr_2O_4$	950 °C	1250 °C	No

[a]Indicates that MnO was used as starting material as opposed to MnO_2 and thus did not require a calcination.

12 different compositions of the form AB_2O_4 (where $A = 5$ equal amounts of Mg, Mn, Fe, Co, Ni, Cu, Zn, and $B =$ Cr or Fe) and $(X)_3O_4$ (where $X = 5$ equal amounts of Mg, Cr, Mn, Fe, Co, Ni, Cu), nine of which achieved single phase and were further characterized. Atomic species components were primarily selected to ensure similar cationic radii and since high-temperature treatments and quenching can achieve optimal oxygen content in the final material, the oxidation state of the chemical precursors was not considered [15]. In this work, we seek to develop mechanisms to tune HEOs through changes in their compositional elements. There is an untapped potential that is starting to be explored to see what can and cannot be stabilized and what functionalities are present and worth pursuing.

II. EXPERIMENTAL

Samples were synthesized from precursor powders of MgO, NiO, CoO, CuO, ZnO, MnO_2, Fe_2O_3, Al_2O_3, Cr_2O_3 of at least 99.95% purity. Oxides were dried in a warming oven for 1 hour to remove any moisture and weighed to stoichiometric proportions. Small 5-gram batches of each composition were ball milled for 60 minutes in a SPEX 8000M Mixer/Mill. Samples were pressed into ½-inch pellets using a die and Carver Uniaxial Press under 3 metric tons of force. Samples were then heat treated per the details in Table I, with the calcination performed using a 5 °C/min ramp and cool rate with a 10-hour dwell time and the sintering with a 5 °C/min ramp rate, 10-hour dwell time and furnace cool. Calcination was performed in order to change the manganese oxide oxidation state to allow for sintering at higher temperature without melting. If after the first sintering the sample was not a single phase, the sample was ground, repressed, and sintered again (up to three times) to achieve phase purity as determined with x-ray diffraction. The structure of each of the samples was determined from x-ray diffraction (XRD) using a PANalytic Empyrean diffractometer setup in Bragg-Brentano geometry utilizing a PIXcel^{3D} area detector with a Cu-Kα source on powder from grinding the polycrystal pellets. Microscopy of the sample surface was performed using a ZEISS EVO scanning electron microscope (SEM) with Bruker xFlash 6130 energy dispersive x-ray spectrometer (EDXS). High-temperature magnetometry measurements from 300–850 K were performed using a Quantum Design VersaLab with vibrating sample magnetometer (VSM), while low-temperature measurements 3–300 K were performed with a Quantum Design Magnetic Property Measurement System (MPMS) with VSM. The low-temperature magnetization sequence was performed in the following method on rounded pieces from the polycrystalline pellets [16]. For the zero-field-cooled (ZFC) measurement the sample was cooled in a zero field from room temperature. The magnetic field was then applied and the magnetization is measured as a function of temperature in warming. The field-cool-cooling (FC) curve is then obtained from measuring the magnetization while cooling to low temperature in the same field. With the same field still applied the field-cooled-warming (FW) curve is obtained from then measuring magnetization while warming from low temperatures back up. Chemical valence and antiferromagnetic ordering were determined using element-specific x-ray absorption spectroscopy (XAS) and magnetic linear dichroism (XMLD) measurements, performed at the Advanced Light Source (ALS) on Beamline 4.0.2. Signal was captured from the total electron yield (TEY) channel, with the x rays incident on the sample.

III. RESULTS/DISCUSSION

The investigated elemental combinations were chosen primarily on the basis of cation radius compatibility. See Table S1 in Ref. [19] for information from the table of Shannon radii and Figs. S1–S5 for some Rietveld refined spectra and Table S2 for lattice parameters and refinement parameters for the fit [17–19]. The twelve compositions studied and their processing temperatures are summarized in Table I. Compositions listed that showed single-phase purity were confirmed with x-ray diffraction spectra alignment with spinel $Fd\text{-}3m$ structure. The $(Mn_{0.2}Fe_{0.2}Co_{0.2}Ni_{0.2}Cu_{0.2})_3O_4$ and $(Mn_{0.2}Fe_{0.2}Co_{0.2}Ni_{0.2}Cu_{0.2})Cr_2O_4$ compositions had remnant metal oxide phase present. The $(Mg_{0.2}Fe_{0.2}Co_{0.2}Ni_{0.2}Cu_{0.2})_3O_4$ composition pellet had surface irregularities and did not achieve a single phase. The XRD diffraction patterns

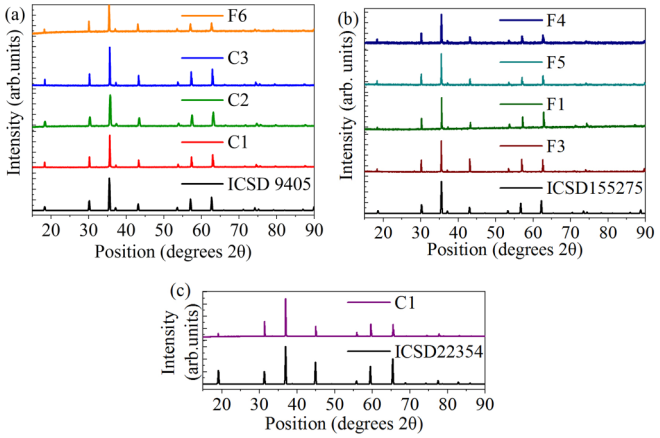

FIG. 1. X-ray diffraction for single-phase HEO spinel compositions that are (a) chromium base with ICSD 9405 $NiCrMnO_4$ d, (b) iron based with ICSD 155275 $MnFe_2O_4$, and (c) aluminum based compared with ICSD 22354 $MgAl_2O_4$ reference patterns showing single-phase spinel Fd-$3m$ structure.

for the nine remaining compositions are shown in Fig. 1 and confirms each is a single phase with a Fm-$3m$ spinel structure.

Energy dispersive x-ray spectroscopy (EDXS) mapping, Fig. 2 (a), shows that the sample possesses a homogenous elemental distribution with no tendency towards segregation. SEM micrographs of $(Mg_{0.2}Fe_{0.2}Co_{0.2}Ni_{0.2}Cu_{0.2})Cr_2O_4$ and $(Mg_{0.2}Co_{0.2}Ni_{0.2}Cu_{0.2}Zn_{0.2})Fe_2O_4$ pellets are shown in Figs. 2 (b) and 2(c), respectively. These images show that these samples have substantial differences in microstructure, with the Fe-based spinel having large, highly interconnected grains, while the Cr-based oxides have a much finer grain structure. See Figs. S10 and S11 for crystallite size calculations and additional EDXS mapping [19].

A spinel distribution can be described by $(A_{1-x}B_x)[A_{x/2}B_{1-x/2}]_2O_4$ with parentheses denoting tetrahedral site and brackets denoting octahedral site with $x = 0$ being a normal spinel, $x = 1$ an inverse, and $x = 2/3$ a completely random solution. In a normal spinel such as $MgAl_2O_4$, The 2^+ cation occupies the tetrahedral A site, while both 3^+ ions occupy the octahedral sites so that it is of the form $(Mg^{2+})[Al^{3+}Al^{3+}]O_4$. In the case of an inverse spinel such as $NiFe_2O_4$, the occupational preference is such that the cation distribution is $(Fe^{3+})[Ni^{2+}Fe^{3+}]O_4$. Preferential site occupancies for the cation species based off charge is provided in the Supplemental for reference, but the effect of the complexity of the compositions studied in this work should be considered. With this in mind, we next focus on the effect of multicomponent composition on the magnetic properties. Ferrite spinels with a structure $(X^{2+})(Fe^{3+})_2O_4$, typically have the B-site ions antiferromagnetically coupled with no net magnetization, while the unpaired electrons on the A-site ion order collinear relative to the B-site ions. This interaction between A-site and B-site cations gives rise to Neel Ferrimagnetism, collinear spins, with net magnetization sensitivity to the cation distribution over the sites. The A-site ion, having no canceling partner, contributes to the observed magnetism of the ferrite.

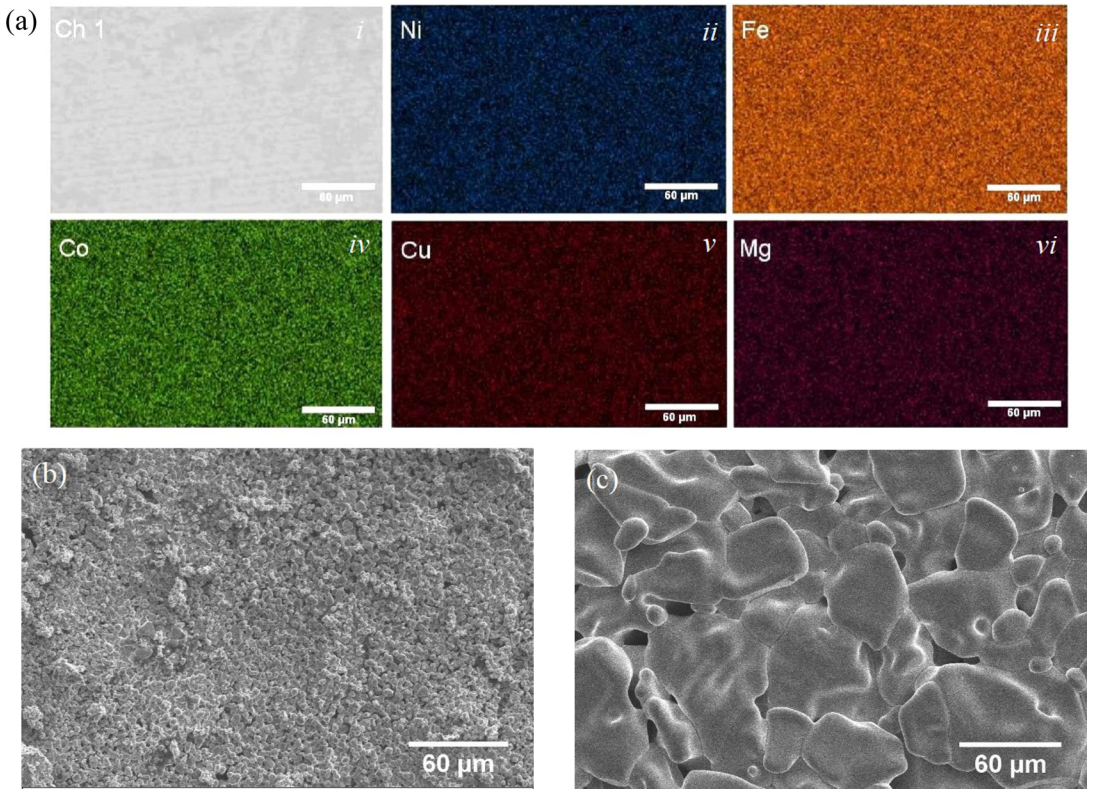

FIG. 2. (a) (i) SEM image of a polished $(Mg_{0.2}Fe_{0.2}Co_{0.2}Ni_{0.2}Cu_{0.2})Fe_2O_4$ pellet and EDXS elemental mapping of the (ii) Ni, (iii) Fe, (iv) Co, (v) Cu, and (vi) Mg distributions. The scale bar indicates 60-μm (b) SEM image of $(Mg_{0.2}Fe_{0.2}Co_{0.2}Ni_{0.2}Cu_{0.2})Cr_2O_4$ pellet and (c) SEM image of $(Mg_{0.2}Co_{0.2}Ni_{0.2}Cu_{0.2}Zn_{0.2})Fe_2O_4$ pellet that was sintered, ground, pressed, and resintered.

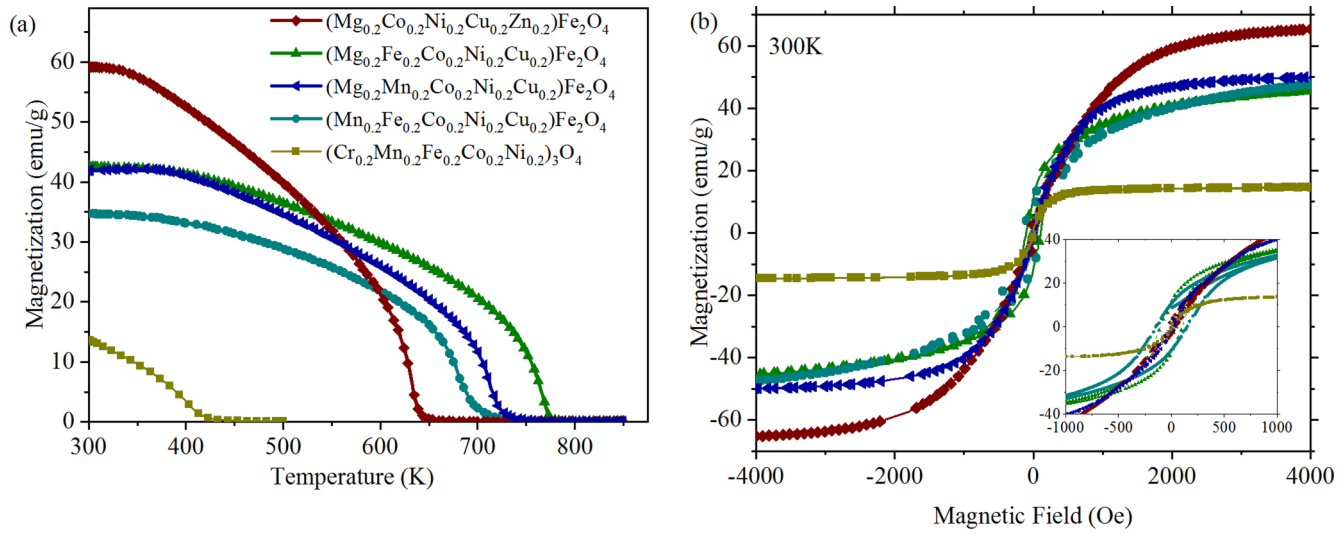

FIG. 3. (a) Field-cooled magnetization of ferritic HEO spinels from 300–850 K with applied field of 1000 Oe and (b) magnetization as a function of applied field at 300 K with inset showing hysteretic behavior (1 emu $= 10^{-3}$ Am^2). The legend in (a) applies to both figures.

Introducing highly disordered *A*-site occupancy will naturally setup a local distribution in the magnetization. Complicating this picture is the change in occupancy of the *A*-site ions when substituting the Fe^{3+} ions causing an imbalance in the antiferromagnetism, generating an additional magnetic moment. This is known to occur when the *A*-site ion is small, as is the case for the elements Mg and Zn. In ferritic spinels these such additions are known to increase the magnetization, due to its preference of tetrahedral site occupancy and the resultant change in the net magnetic moment, and decrease the transition temperature [20–23]. Furthermore, the filled s and d-shells of Mg and Zn means they do not contribute to the magnetism, maximizing the asymmetry, but also causing a reduction in the Néel Temperature, T_N. Indeed, the HEOs incorporating both Zn and Mg show the largest moment and have the lowest T_N relative to the other HEOs, as shown in Fig. 3(a). The ferrites with only Mg show the next-largest saturation moment and a higher T_N, where T_N is the high-temperature ferrimagnetic to paramagnetic transition temperature. Finally, the ferrite without either Mg or Zn has the smallest moment, but also a lower T_N. This indicates some site preference trends are maintained. These results emphasize the crucial role played by the antiferromagnetic ordering on the *B* site, in that even fractional substitution causes significant changes in T_N. This sentiment is further emphasized in the HEO without a preferred *B*-site occupancy, which shows a significantly suppressed T_N and magnetic moment. Note that all of the T_N are above room temperature.

The room temperature magnetization with magnetic field measured on each of the HEOs were measured at 300 K and are presented in Fig. 3(b). These measurements show a narrow coercivity for each of the samples, with saturation fields of >4 kOe(1 kOe $= 0.1$ T). The hysteretic behavior confirms the ferrimagnetic behavior expected for these materials. The large saturation field may indicate local regions that are mutually antiferromagnetically coupled or possess large magnetocrystalline anisotropy.

Magnetometry measurements performed on $(Cr_{0.2}Mn_{0.2}Fe_{0.2}Co_{0.2}Ni_{0.2})_3O_4$ are shown in Fig. 4. The ZFC plot shows a series of inflections, potentially indicating the onset of ordering of various regions within the sample. The direct exchange interaction, which exists only between two neighboring atoms, is intrinsically localized. Specifically, statistical fluctuations may cause regions to be particularly rich in a specific element at a local level, resulting in a localized variation in T_N. Alternatively, local atomic regions particularly rich in Cr or Mn may possess an antiferromagnetic to ferromagnetic transition, resulting from their negative exchange coupling with the other constituent elements. This hypothesis is further supported by the FC and FW plots in Fig. 4(a) which show a peak in the plot at 230 K, where the magnetization is in-fact decreasing with decreasing temperature, and by the small magnetization in this sample shown in Fig. 3(a). Magnetic hysteresis loops were also measured and show an increase in coercivity with decreasing temperature—as would be expected for thermally activated reversal. However, the scale of the coercivity's thermal dependence is notable for a bulk material, increasing from 20 Oe at 300 K to 197 Oe at 50 K. This is likely a consequence of the large site-specific T_N, resulting from the compositional distribution.

Figure 5 shows the low-temperature magnetization of two ferrite-based HEO spinels, $(Mg_{0.2}Mn_{0.2}Co_{0.2}Ni_{0.2}Cu_{0.2})Fe_2O_4$ and $(Mg_{0.2}Fe_{0.2}Co_{0.2}Ni_{0.2}Cu_{0.2})Fe_2O_4$, revealing interesting magnetic behavior with (i) the FW data dipping below the FC plot, and (ii) a reduction in magnetization with decreasing temperature. This again could be due to an antiferromagnetic coupling between neighboring elemental components. These minority phases may be frozen upon cooling, and persist upon warming, exhibiting a thermal hysteresis, and explaining the crossover.

While the ferrite spinels show features typical of ferro—or ferri—magnetic behavior, the chrome-based spinels are notably different. The ZFC magnetization versus temperature for the chromates, shown in Fig. 6, increases from low temperatures and approaches a maximum before decreasing upon further increasing temperatures. This feature is well known and associated with superparamagnetic behavior, with the maximum called the blocking temperature (T_B) [24].

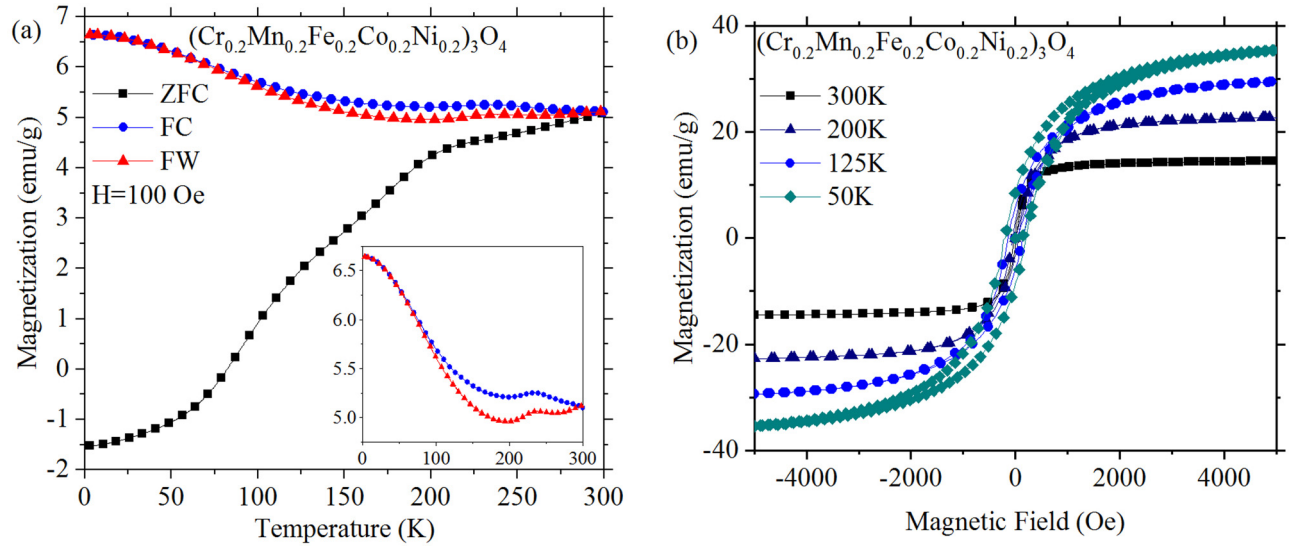

FIG. 4. Direct-current magnetization for $(Cr_{0.2}Mn_{0.2}Fe_{0.2}Co_{0.2}Ni_{0.2})_3O_4$ (a) as a function of temperature from 3–300 K showing the zero field-cooled (ZFC), field-cooled, measured while cooling (FC) and field-cooled, measured while warming (FW) plots; field-cooled measurements were performed with an applied field of 100 Oe. (b) Magnetic hysteresis loops measured at 300, 200, 125, and 50 K.

Superparamagnetism arises due to the magnetic interaction volume and anisotropy being smaller than the thermal fluctuations. Thus the presence of a blocking temperature indicates that the magnetic regions within the sample are small and relatively isolated. Estimating that the magnetic anisotropy is approximately similar to ferrite spinels (18.7×10^{-3} J/m^3), the diameter of the magnetic regions can be estimated as ≈7.3 nm [25]. The FC data show an increase in the magnetization with increasing field, which is not typical for superparamagnetic materials, but simply indicates that there may be some residual regions with antiferromagnetic ordering at room temperature [10].

The magnetization curves in Figs. 6(a)–6(c) show slight dips approaching T_B as well as different character at the antiferromagnetic onset approaching T_N. There is also a field dependence seen in the magnetization curves. This could be explained by ferromagnetic contributions to the lattice. This was noted as a possible factor in the recent HEO perovskite magnetic investigation where small ferromagnetic contributions are distinguished amidst predominantly antiferromagnetic behavior possibly due to small ferromagnetic clusters or configurations within the antiferromagnetic matrix [10]. In a disordered material, especially ones such as these with multiple magnetic constituents, homogeneity at the atomic level is not assumed. Local variations could give rise to small ferromagnetic clusters, small pockets of slightly differently ordered spins within a larger overall ordering. Ferrimagnetic contributions are further supported by the mirror-like symmetry in

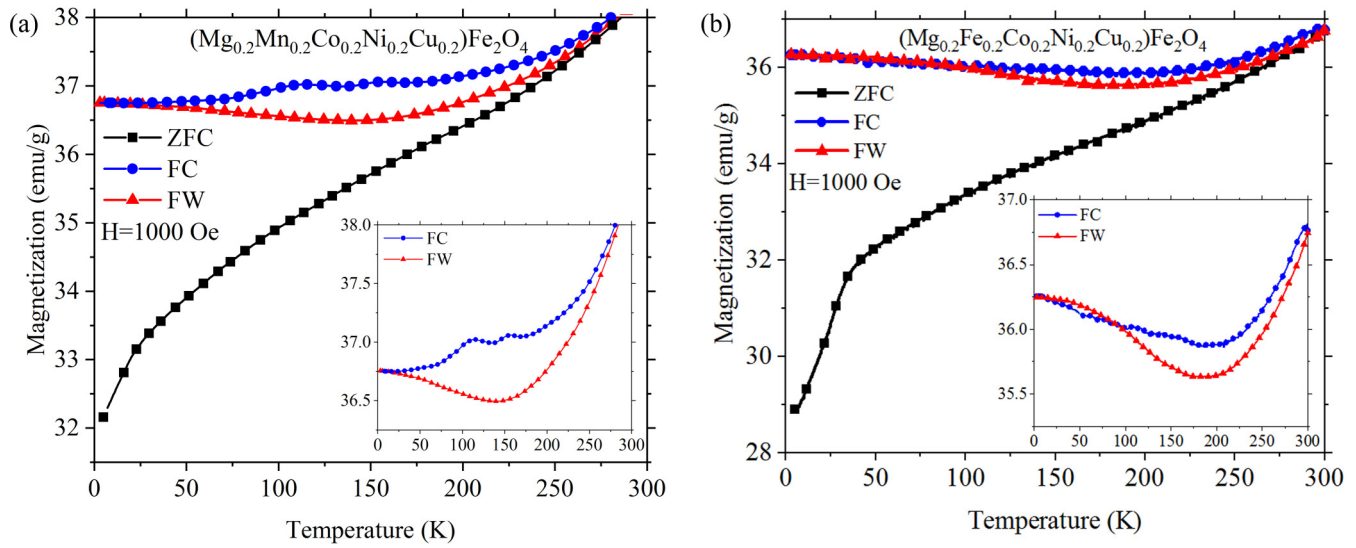

FIG. 5. Direct-current magnetization as a function of temperature from 3–300 K showing the zero field-cooled (ZFC), and field-cooled plots, measured in 100 Oe, measured along the cooling (FC) and warming (FW) branches for (a) $(Mg_{0.2}Mn_{0.2}Co_{0.2}Ni_{0.2}Cu_{0.2})Fe_2O_4$ and (b) $(Mg_{0.2}Fe_{0.2}Co_{0.2}Ni_{0.2}Cu_{0.2})Fe_2O_4$. Inset plots are provided to emphasize the cross-over and hysteresis in the FC and FW plots.

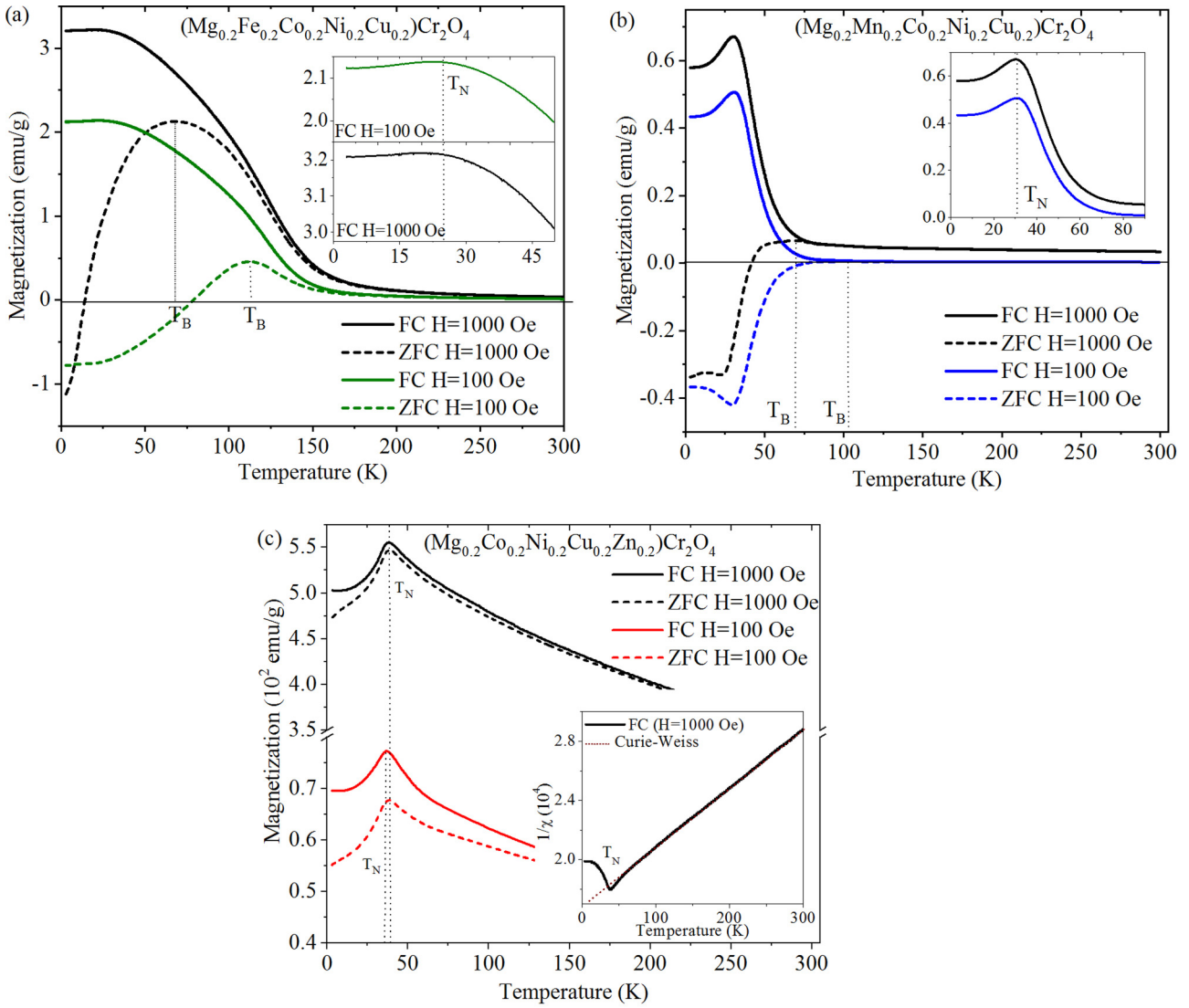

FIG. 6. Low-temperature dc magnetization from 3–300 K under 100 and 1000 Oe for (a) $(Mg_{0.2}Fe_{0.2}Co_{0.2}Ni_{0.2}Cu_{0.2})Cr_2O_4$, (b) $(Mg_{0.2}Mn_{0.2}Co_{0.2}Ni_{0.2}Cu_{0.2})Cr_2O_4$ with inset of field-cooled inverse susceptibility with temperature under a field of 1000 Oe for $(Mg_{0.2}Co_{0.2}Ni_{0.2}Cu_{0.2}Zn_{0.2})Cr_2O_4$. (c) Low-temperature dc magnetization from 3–300 K under 100 and 1000 Oe for $(Mg_{0.2}Co_{0.2}Ni_{0.2}Cu_{0.2}Zn_{0.2})Cr_2O_4$.

the FC- ZFC behavior in $(Mg_{0.2}Mn_{0.2}Co_{0.2}Ni_{0.2}Cu_{0.2})Cr_2O_4$ shown in Fig. 6(b) as this symmetry is typical for materials containing a ferromagnetic component [26]. The inverse susceptibility of $(Mg_{0.2}Co_{0.2}Ni_{0.2}Cu_{0.2}Zn_{0.2})Cr_2O_4$ shown in the inset of Fig. 6(c) shows more classical Curie-Weiss-like behavior, with low-temperature antiferromagnetic ordering at $T_N = 36$ K. The blocking temperatures can be identified at 100 Oe and 1000 Oe to be ≈38.1 and ≈39 K for $(Mg_{0.2}Co_{0.2}Ni_{0.2}Cu_{0.2}Zn_{0.2})Cr_2O_4$, ≈69 and ≈112.2 K for $(Mg_{0.2}Fe_{0.2}Co_{0.2}Ni_{0.2}Cu_{0.2})Cr_2O_4$, and ≈102.2 and ≈69 K for $(Mg_{0.2}Mn_{0.2}Co_{0.2}Ni_{0.2}Cu_{0.2})Cr_2O_4$, respectively.

Magnetization versus magnetic field for $(Mg_{0.2}Fe_{0.2}Co_{0.2}Ni_{0.2}Cu_{0.2})Cr_2O_4$ and $(Mg_{0.2}Mn_{0.2}Co_{0.2}Ni_{0.2}Cu_{0.2})Cr_2O_4$ was measured using a Quantum Design Physical Property Measurement System (PPMS) DynaCool with VSM. Hysteresis of $(Mg_{0.2}Fe_{0.2}Co_{0.2}Ni_{0.2}Cu_{0.2})Cr_2O_4$ is shown in Fig. 7 and has a saturation field of ∼5 T at 30 K with the coercive force increasing towards 1.9 K, but without any changes in the saturation behavior. For $(Mg_{0.2}Mn_{0.2}Co_{0.2}Ni_{0.2}Cu_{0.2})Cr_2O_4$, there is a lack of saturation even at 9-T fields. In Fig. 8, an exchange bias is seen increasingly at lower temperature. Increasing coercivity with decrease in temperature is indicative of thermally activated reversal and was expected, however at lower temperature the coercivity diverges and narrows as depicted by the behavior at 1.9 K. Just as seen in Fig. 7; in Fig. 8, there is no decrease in the magnetic saturation which in this case would have been expected to occur in correlation with the coercivity divergence. These behaviors could indicate more complex changes in the ordering at the transitions identified in Fig. 6. Exchange coupling as well as small localized antiferromagnetic contributions and antiferromagnetic stability could be contributing to an increase in coercivity. In a recent study on $(Mg_{0.25(1-x)}Co_xNi_{0.25(1-x)}Cu_{0.25(1-x)}Zn_{0.25(1-x)})O$ heterostructures with changes in Co concentration, anisotropic

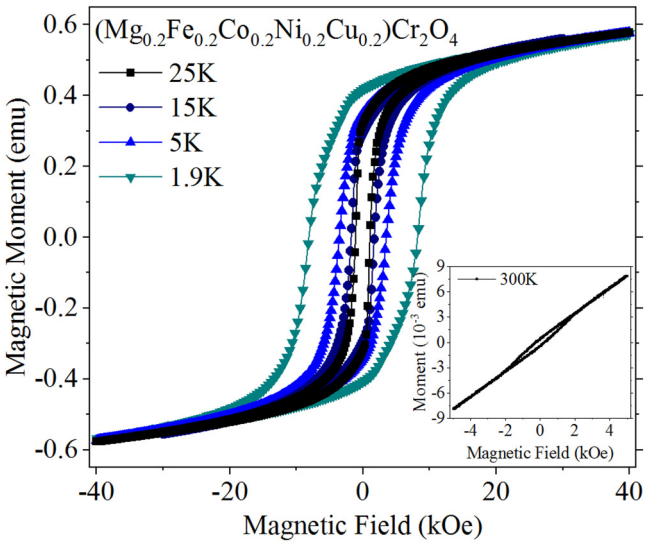

FIG. 7. The hysteresis plots at 25, 15, 5, and 1.9 K for $(Mg_{0.2}Fe_{0.2}Co_{0.2}Ni_{0.2}Cu_{0.2})Cr_2O_4$ with inset showing behavior at 300 K.

magnetic exchange and the presence of a critical blocking temperature was observed, indicating antiferromagnetic order with composition changes tuning the disorder, exchange field and magnetic anisotropy [8]. Magnetization with magnetic field plots for $(Mg_{0.2}Ni_{0.2}Co_{0.2}Cu_{0.2}Zn_{0.2})Cr_2O_4$, $(Mg_{0.2}Mn_{0.2}Co_{0.2}Ni_{0.2}Cu_{0.2})Fe_2O_4$ and $(Mg_{0.2}Fe_{0.2}Co_{0.2}Ni_{0.2}Cu_{0.2})Fe_2O_4$ are provided in Figs. S7 and S8 [19].

As summarized in Table II, the ferritic HEO spinels maintain ferrimagnetic character to very high temperature, while the chromium-based compositions have low-temperature magnetic ordering, with T_N well below room temperature. Transition temperatures reported in literature in polycrystalline traditional spinel materials are referenced providing a basis of comparison to those reported in our work. As the table shows, depending on the *A*-site and *B*-site cations in traditional spinels, the constituents lead to different types and temperature ranges of magnetic transitions. Using the multicomponent approach to material design could move toward developing the tunability these entropic spinels have the possibility of achieving.

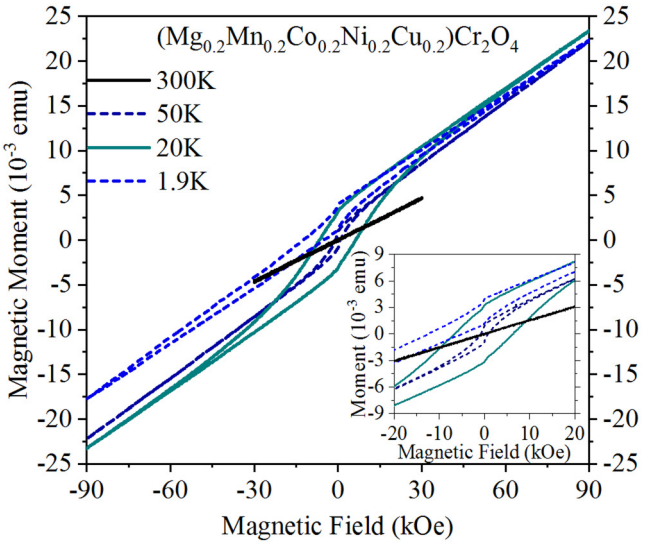

FIG. 8. Magnetization with field of $(Mg_{0.2}Mn_{0.2}Co_{0.2}Ni_{0.2}Cu_{0.2})Cr_2O_4$ at 300, 50, 20, and 1.9 K with inset better showing hysteresis.

The measurements presented above have captured the bulk features of a system with extremely localized chemical and likely magnetic disorder. To fingerprint the magnetic ordering and chemical environment of each of the constituent elements, XAS and XMLD were used. An example case, measuring the Cr and Fe L_3 and L_2 edges of $(Mg_{0.2}Fe_{0.2}Co_{0.2}Ni_{0.2}Cu_{0.2})Cr_2O_4$ at 20 and 300 K, is shown in Fig. 9. At 20 K [Fig. 9(a)], the Cr XMLD signal is weak, but shows a clear positive/negative inflection, strongly suggesting that the Cr is antiferromagnetically coupled—as expected on the octahedral *B* site. Increasing the temperature to 300 K, the XMLD signal disappears, indicating that the *B*-site ion is no-longer antiferromagnetically coupled. This is consistent with the magnetization data discussed above, which show magnetic transitions at 23 and 146 K. XMLD measurements were also performed on the Fe element and show antiferromagnetic ordering to at least room temperature. This may indicate Fe substitution for Cr on the *B* site in this composition. The XMLD signal can also arise due to orbital polarization, in this case induced by symmetry breaking at the surface, however, we would not expect a strong temperature dependence of this effect, which is observed here. This supports that the origin of the XMLD is antiferromagnetic ordering. XMLD measurements performed on the ferrites confirmed the antiferromagnetic ordering on the *B* site at 20 and 300 K for both of the tested samples, $(Mg_{0.2}Mn_{0.2}Co_{0.2}Ni_{0.2}Cu_{0.2})Fe_2O_4$, and $(Mn_{0.2}Fe_{0.2}Co_{0.2}Ni_{0.2}Cu_{0.2})Fe_2O_4$.

Valence information is determined from the XAS measurement for $(Mg_{0.2}Fe_{0.2}Co_{0.2}Ni_{0.2}Cu_{0.2})Cr_2O_4$, indicating an unexpected mixed state, with Cr^{3+}/Cr^{4+}. Interestingly, the Cr valence *increases* with temperature, starting at $Cr^{3.55+}$ at 20 K, and increasing to $Cr^{3.65+}$ at 300 K; error on the valence is ± 0.03, as determined by the weighting necessary to reduce the quality of the fit by one standard deviation. The valence increase can be qualitatively inferred from the XAS spectra, Fig. 9. Specifically, between 20 and 300 K the features on the low-energy side of the L_3 peak are suppressed, while a new shoulder emerges on the high-energy side. The XAS of the Fe in the $(Mg_{0.2}Fe_{0.2}Co_{0.2}Ni_{0.2}Cu_{0.2})Cr_2O_4$ shows a mixed Fe^{2+}/Fe^{3+} state, and a decrease in valence (from $Fe^{2.29+}$ to $Fe^{2.15+}$) with increasing temperatures, with the decrease in the Fe valence complementing the increase in the Cr. This shows that the chromium valence increases towards 4+ with temperature while the iron valence decreased towards 2+ with increasing temperature. Chromium containing spinel oxides are expected to possess a mixed Cr^{2+}/Cr^{3+} state, so the presence of Cr^{4+} is unique [12,34]. In spinels where $A = 2^+$ and $B = 3^+$ (2,3 spinels) there is a preference for the larger ion to occupy the tetrahedral site, while in 2–4 spinels ($A = 4^+$ and $B = 2^+$) the opposite holds true with larger ions preferring the octahedral site [34].

XAS and XMLD of the Fe and Mn ions in $(Mg_{0.2}Mn_{0.2}Co_{0.2}Ni_{0.2}Cu_{0.2})Fe_2O_4$ was also measured (not shown). These measurements confirm the expected

TABLE II. Summary of transition temperature for investigated HEO spinel compositions and those from literature for individual iron- and chromium-based polycrystalline spinels for comparison. Note that for the Ferritic spinels, T_N indicates the ferrimagnetic to paramagnetic high-temperature transition. For chromium-based spinels, T_N is the onset of change in magnetic ordering with F = ferrimagnetic and AF = antiferromagnetic.

Composition	T_N (K)	Composition	$\sim T_N$ (K)
$(Mg_{0.2}Fe_{0.2}Co_{0.2}Ni_{0.2}Cu_{0.2})Fe_2O_4$	774	$(Mg_{0.2}Co_{0.2}Ni_{0.2}Cu_{0.2}Zn_{0.2})Cr_2O_4$	AF:36
$(Mg_{0.2}Mn_{0.2}Co_{0.2}Ni_{0.2}Cu_{0.2})Fe_2O_4$	735	$(Mg_{0.2}Fe_{0.2}Co_{0.2}Ni_{0.2}Cu_{0.2})Cr_2O_4$	F: 146 AF:23
$(Mn_{0.2}Fe_{0.2}Co_{0.2}Ni_{0.2}Cu_{0.2})Fe_2O_4$	715	$(Mg_{0.2}Mn_{0.2}Co_{0.2}Ni_{0.2}Cu_{0.2})Cr_2O_4$	F: 70 AF:30
$(Mg_{0.2}Co_{0.2}Ni_{0.2}Cu_{0.2}Zn_{0.2})Fe_2O_4$	648		
$(Cr_{0.2}Mn_{0.2}Fe_{0.2}Co_{0.2}Ni_{0.2})_3O_4$	425	$CoCr_2O_4$ [27]	F: 97 AF: 27,15
Fe_3O_4 [28]	858	$NiCr_2O_4$ [27]	F: 75 AF: 31
$CoFe_2O_4$ [28]	793	$MnCr_2O_4$ [27]	F: 43 AF: 18, 15
$MgFe_2O_4$ [29]	590	$MgCr_2O_4$ [30]	AF: 12.5
$NiFe_2O_4$ [28]	860	$CuCr_2O_4$ [30]	F: 128
$MnFe_2O_4$ [28]	577	$ZnCr_2O_4$ [31]	AF: 12
$CuFe_2O_4$ [28]	728	$FeCr_2O_4$ [32]	F: 93
$ZnFe_2O_4$ [33]	460		

mixed Fe^{3+}/Fe^{2+} and mixed Mn^{3+}/Mn^{2+} valence. At 20 K, the valences are found to be $Fe^{2.96+}$ and $Mn^{2.11+}$, the XMLD showing antiferromagnetic ordering in the Fe and seemingly no magnetic ordering in the Mn. Increasing the temperature to 77 and 300 K increases the Mn valence to $Mn^{2.25+}$ and $Mn^{2.42+}$ and decreases the Fe valence to $Fe^{2.81+}$ and $Fe^{2.43+}$, respectively. The larger $Fe^{2.96+}$ valence at low-temperature is partly expected at lower temperatures

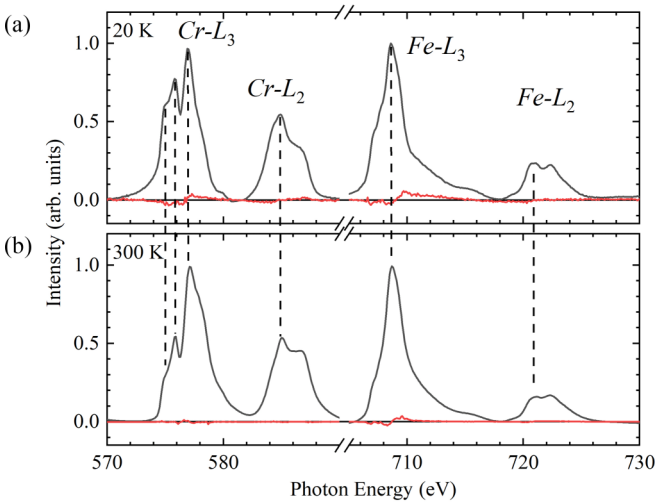

FIG. 9. Cr and Fe x-ray absorption spectroscopy (XAS) spectra with x-ray magnetic linear dichroism (XMLD) signal given by red line at (a) 300 and (b) 20 K for polycrystalline $(Mg_{0.2}Fe_{0.2}Co_{0.2}Ni_{0.2}Cu_{0.2})Cr_2O_4$.

to help stabilize the d^5 configuration, but more importantly due to the 2+ preference of the Mn, Ni, and Co cations. These coupled changes in valence are similar to the chromate case and illustrate a balancing of the electrons in the system. The XMLD measurements shows strong antiferromagnetic ordering in the Fe site at 20 and 77 K, but only weak, noise-level XMLD signal at 300 K; the Mn XMLD shows no antiferromagnetic ordering at any temperature. A similar trend was seen in $(Mn_{0.2}Fe_{0.2}Co_{0.2}Ni_{0.2}Cu_{0.2})Fe_2O_4$ with the Fe valence decreasing with increasing temperature with antiferromagnetic ordering at low temperature and no discernable antiferromagnetic ordering at room temperature. The valence information for these three samples is summarized in Table S3 [19]. Valence changes in spinel systems often tie to lattice inversion and site occupancy changes with temperature. As these compositions are novel, the mechanism of valence change with temperature is not yet clear but could be due to electron delocalization.

IV. CONCLUSION

A family of new HEO materials are synthesized, and bulk structural and magnetic properties are reported, showing low-temperature antiferromagnetic ordering in some ferritic and in all chromium based spinels and high-temperature ferrimagnetic transition in ferritic HEO spinels. Blocking temperatures are found for $(Mg_{0.2}Fe_{0.2}Co_{0.2}Ni_{0.2}Cu_{0.2})Cr_2O_4$, $(Mg_{0.2}Mn_{0.2}Co_{0.2}Ni_{0.2}Cu_{0.2})Cr_2O_4$, and $(Mg_{0.2}Co_{0.2}Ni_{0.2}Cu_{0.2}Zn_{0.2})Cr_2O_4$. While the exact mechanism for the magnetic behavior seen is not yet understood in these

materials, some theories and supporting literature are stated as well as contributing factors. Field-cooled and field-warmed hysteresis is seen in $(Mg_{0.2}Mn_{0.2}Co_{0.2}Ni_{0.2}Cu_{0.2})Fe_2O_4$, $(Mg_{0.2}Fe_{0.2}Co_{0.2}Ni_{0.2}Cu_{0.2})Fe_2O_4$, and $(Cr_{0.2}Mn_{0.2}Fe_{0.2}Co_{0.2}Ni_{0.2})_3O_4$. X-ray absorption measurements showed valence trends with temperature for $(Cr_{0.2}Mn_{0.2}Fe_{0.2}Co_{0.2}Ni_{0.2})_3O_4$, $(Mg_{0.2}Mn_{0.2}Co_{0.2}Ni_{0.2}Cu_{0.2})Fe_2O_4$ as well as the finding of Cr^{4+} presence in $(Mg_{0.2}Fe_{0.2}Co_{0.2}Ni_{0.2}Cu_{0.2})Cr_2O_4$, along with indications of some degree of low-temperature antiferromagnetic ordering in all three compositions. While the magnetic structure's complexity and multitude of magnetic species comes with inherent difficulty to solve, entropic systems offer another avenue for further tuning of magnetic properties and expansion of the understanding and capabilities of multicomponent systems. Further work to interrogate the local structure of this new HEO material class is needed for better fundamental understanding and growth towards functionality.

ACKNOWLEDGMENTS

B.M. acknowledges the support of the Center for Materials Processing, a Tennessee Higher Education Commission (THEC) supported Accomplished Center of Excellence. Powder XRD and Microscopy was performed at the Joint Institute for Advanced Materials (JIAM) Diffraction Facility and Microscopy Facility, located at the University of Tennessee, Knoxville. Magnetic characterization supported by the US Department of Energy (DOE), Office of Science, Basic Energy Sciences, Materials Sciences and Engineering Division. This research used resources of the Advanced Light Source, which is a DOE Office of Science User Facility under Contract No. DE-AC02-05CH11231. Certain trade names and company products are identified to specify adequately the experimental procedure. In no case does such identification imply recommendation or endorsement by the National Institute of Standards and Technology, nor does it imply that the products are necessarily the best for the purpose.

[1] J. W. Yeh *et al.*, Nanostructured high-entropy alloys with multiple principal elements: Novel alloy design concepts and outcomes, Adv. Eng. Mater. **6**, 299 (2004).

[2] C. M. Rost *et al.*, Entropy-stabilized oxides, Nat. Commun. **6**, 8485 (2015).

[3] S. Jiang *et al.*, A new class of high-entropy perovskite oxides, Scr. Mater. **142**, 116 (2018).

[4] A. Sarkar *et al.*, Rare earth and transition metal based entropy stabilised perovskite type oxides, J. Eur. Ceram. Soc. **38**, 2318 (2018).

[5] J. Gild *et al.*, High-entropy fluorite oxides, J. Eur. Ceram. Soc. **38**, 3578 (2018).

[6] K. Chen *et al.*, A five-component entropy-stabilized fluorite oxide, J. Eur. Ceram. Soc. **38**, 4161 (2018).

[7] Y. Sharma *et al.*, Single-crystal high entropy perovskite oxide epitaxial films, Phys. Rev. Mater. **2**, 060404 (2018).

[8] P. B. Meisenheimer, T. J. Kratofil, and J. T. Heron, Giant enhancement of exchange coupling in entropy-stabilized oxide heterostructures, Sci. Rep. **7**, 13344 (2017).

[9] R. Witte *et al.*, High-entropy oxides: An emerging prospect for magnetic rare-earth transition metal perovskites, Phys. Rev. Mater. **3**, 034406 (2019).

[10] E. C. Abenojar, S. Wickramasinghe, J. Bas-Concepcion, and A. C. S. Samia, Structural effects on the magnetic hyperthermia properties of iron oxide nanoparticles, Prog. Nat. Sci. Mater. Int. **26**, 440 (2016).

[11] T. C. Arnoldussen and E.-M. Rossi, Materials for magnetic recording, Annu. Rev. Mater. Sci. **15**, 379 (2003).

[12] R. J. Hill, J. R. Craig, and G. V. Gibbs, Systematics of the spinel structure type, Phys. Chem. Miner. **4**, 317 (1979).

[13] J. Dąbrowa *et al.*, Synthesis and microstructure of the $(Co, Cr, Fe, Mn, Ni)_3O_4$ high entropy oxide characterized by spinel structure, Mater. Lett. **216**, 32 (2018).

[14] A. Mao, F. Quan, H. Xiang, Z. Zhang, and K. Kuramoto, Facile synthesis and ferrimagnetic property of spinel $(CoCrFeMnNi)_3O_4$ high-entropy oxide nanocrystalline powder, J. Mol. Struct. **1194**, 11 (2019).

[15] D. Bérardan, S. Franger, D. Dragoe, A. K. Meena, and N. Dragoe, Colossal dielectric constant in high entropy oxides, Phys. Status Solidi - Rapid Res. Lett. **10**, 328 (2016).

[16] Y. Liu, D. J. Sellmyer, and D. Shindo, *Handbook of Advanced Magnetic Materials* (Springer, New York, 2006).

[17] R. D. Shannon, Revised effective ionic radii and systematic studies of interatomic distances in halides and chalcogenides, Acta Crystallogr. Sect. A **32**, 751 (1976).

[18] B. H. Toby and R. B. Von Dreele, GSAS-II: the genesis of a modern open-source all purpose crystallography software package, J. Appl. Crystallogr. **46**, 544 (2013).

[19] See Supplemental Material at http://link.aps.org/supplemental/10.1103/PhysRevMaterials.3.104416 for cation constituent information, Rietveld refined XRD spectra and lattice values, additional EDXS mapping, summary of valence information and additional magnetic characterization.

[20] D. S. Birajdar, D. R. Mane, S. S. More, V. B. Kawade, and K. M. Jadhav, Structural and magnetic properties of $Zn_xCu_{1.4-x}Mn_{0.4}Fe_{1.2}O_4$ ferrites, Mater. Lett. **59**, 2981 (2005).

[21] M. Rana, M. Islam, and T. Abbas, Cation distribution and magnetic interactions in Zn-substituted $CuFe_2O_4$ ferrites, Mater. Chem. Phys. **65**, 345 (2000).

[22] H. El Moussaoui, R. Masrour, O. Mounkachi, M. Hamedoun, and A. Benyoussef, Cation distribution and magnetic interactions in ZN-substituted $Fe(Cu)Fe_2O_4$ ferrites, J. Supercond. Nov. Magn. **25**, 2473 (2012).

[23] S. A. Mazen, S. F. Mansour, and H. M. Zaki, Some physical and magnetic properties of Mg-Zn ferrite, Cryst. Res. Technol. **38**, 471 (2003).

[24] B. D. Cullity and C. D. Graham, *Introduction to Magnetic Materials*, 2nd ed (Wiley, Hoboken, NJ, 2009).

[25] L. Rebbouh *et al.*, Characterization and magnetic properties of core/shell structured Fe/Au nanoparticles, J. Appl. Phys. **95**, 6804 (2004).

[26] D. J. Dunlop, Transition warming and cooling remanences in pyrrhotite and hematite, Geophys. J. Int. **203**, 605 (2015).

[27] N. Mufti, A. A. Nugroho, G. R. Blake, and T. T. M. Palstra, Magnetodielectric coupling in frustrated spin systems: The spinels MCr_2O_4 (M = Mn, Co and Ni), J. Phys. Condens. Matter **22**, 2 (2010).

[28] J. Smit and H. P. J. Wijn, *Ferrites* (Wiley, New York, 1959).

[29] M. U. Rana and T. Abbas, Ac susceptibility and magnetic interaction in Mg – Ni – Fe – O system, Mater. Lett. **57**, 925 (2002).

[30] M. C. Kemei, S. L. Moffitt, D. P. Shoemaker, and R. Seshadri, Evolution of magnetic properties in the normal spinel solid solution $Mg_{1-x}Cu_xCr_2O_4$, J. Phys. Condens. Matter **24**, 046003 (2012).

[31] B. C. Melot, J. E. Drewes, R. Seshadri, E. M. Stoudenmire, and A. P. Ramirez, Magnetic phase evolution in the spinel compounds $Zn_{1-x}Co_xCr_2O_4$, J. Phys.: Condens. Matter **21**, 216007 (2009).

[32] K. Singh, A. Maignan, C. Simon, and C. Martin, $FeCr_2O_4$ and $CoCr_2O_4$ spinels: Multiferroicity in the collinear magnetic state? Appl. Phys. Lett. **99**, 172903 (2011).

[33] J. H. Shim, S. Lee, J. H. Park, S.-J. Han, Y. H. Jeong, and Y. W. Cho, Coexistence of ferrimagnetic and antiferromagnetic ordering in Fe-inverted zinc ferrite investigated by NMR, Phys. Rev. B **73**, 064404 (2006).

[34] H. O'Neill and A. Navrotsky, Simple spinels; crystallographic parameters, cation radii, lattice energies, and cation distribution, Am. Mineral. **68**, 181 (1983).